OPEN

Gadolinium-based Contrast Agents Trigger Gadolinium Accumulation Within the Hippocampus In Vivo and Mitochondrial Alterations in Organotypic Hippocampal Tissue Cultures Ex Vivo

Rebecca Ludwig, MD, PhD, Mathias Schannor, PhD, Heike Traub, PhD, Carmen Infante-Duarte, PhD, and Lina Anderhalten, MD, PhD

Background: In multiple sclerosis (MS), mitochondrial dysfunction contributes to disease progression and may impair cognitive function, particularly in vulnerable regions such as the hippocampus. Gadolinium-based contrast agents (GBCAs) are widely used for imaging-based diagnosis of MS; however, evidence indicates that gadolinium (Gd) can be released from low-stability agents and retained in the brain. Whether retained Gd affects neuronal mitochondria, particularly under inflammatory conditions, remains unclear. We investigated hippocampal Gd retention following in vivo GBCA exposure and assessed associated mitochondrial effects in hippocampal slice cultures.

Methods: Mice with experimental autoimmune encephalomyelitis (EAE) and healthy controls received repeated injections of linear gadopentetate-dimeglumine (gadopentetate) or macrocyclic gadobutrol (cumulative dose: 20 mmol/kg body weight). Hippocampal Gd distribution and retention kinetics were analyzed 1, 10, and 40 days post-final injection (p.f.i.) using laser ablation inductively coupled plasma-time-of-flight mass spectrometry (LA-ICP-ToF-MS). Ex vivo, organotypic hippocampal slice cultures from B6.Cg-Tg(Thy1-CFP/COX8A)S2Lich/J mice expressing fluorescently labeled neuronal mitochondria were exposed to TNF-alpha (paradigm of inflammation) ± gadopentetate or gadobutrol for 48 hours (0.1, 1, 10, 50 mM). Mitochondrial dynamics were quantified using semi-automated and manual analyses of confocal microscopy images, and Gd slice content was determined by ICP-MS.

Results: In vivo, neuroinflammation increased hippocampal Gd accumulation following administration of both GBCAs in EAE mice. However, long-term retention up to 40 days p.f.i. was observed exclusively for gadopentetate, particularly in EAE mice. Ex vivo, prolonged exposure to both GBCAs at low-to-intermediate concentrations (0.1 to 10 mM) reduced mitochondrial length and area, particularly under inflammatory conditions, and altered mitochondrial motility relative to untreated controls. At these concentrations, intratissue Gd levels, quantified by ICP-MS under representative conditions, were within a biologically relevant, sub-cytotoxic range. Marked motility impairment and mitochondrial rounding occurred only at the highest gadopentetate concentration (50 mM). Interestingly, although inflammation did not alter Gd concentrations within the ex vivo slices, mitochondrial alterations were more pronounced under inflammatory conditions.

Conclusion: In the hippocampus, long-term Gd retention in vivo appears to be restricted to linear GBCAs, whereas ex vivo, exposure to both linear and macrocyclic GBCAs at biologically relevant concentrations alters neuronal mitochondrial morphology and dynamics. Inflammation further amplifies these effects, highlighting the importance of considering GBCA-associated mitochondrial damage when evaluating their potential neurotoxic risks, particularly in neuroinflammatory diseases.

Key Words: multiple sclerosis, neurodegeneration, neuroinflammation, gadolinium-based contrast agents, mitochondrial toxicity, chronic organotypic hippocampal slice culture, mitochondrial dynamics, live imaging, confocal fluorescence microscopy, inductively coupled plasma mass spectrometry

(*Invest Radiol* 2026;00:000–000)

Multiple sclerosis (MS) is a chronic inflammatory disorder of the central nervous system (CNS) affecting ~2.8 million individuals worldwide.[1] It is characterized by focal inflammatory lesions caused by infiltration of autoreactive immune cells into the CNS, resulting in demyelination and neuroaxonal damage. Clinical symptoms include visual, sensory, motor, and cognitive impairment.[2,3] According to the 2024 McDonald criteria, MS diagnosis requires evidence of lesion dissemination in

Received for publication May 8, 2026; and accepted for publication, after revision, August 23, 2026.

From the Experimental and Clinical Research Center, A Cooperation Between the Max Delbrück Center for Molecular Medicine in the Helmholtz Association and Charité—Universitätsmedizin Berlin, Berlin, Germany (R.L., C.I.D., L.A.); Division Inorganic Trace Analysis, Bundesanstalt für Materialforschung und-prüfung, Berlin, Germany (M.S., H.T.); Institute of Geological Sciences, Freie Universität Berlin, Berlin, Germany (M.S.).

C.I.-D. and L.A. contributed equally.

C.I.-D. and L.A.: conceptualization. R.L. and L.A.: methodology, validation, formal analysis, writing—original draft preparation. R.L. and M.S.: software. R.L., M.S. and L.A.: investigation. R.L.: data curation. M.S., H.T., and C.I.-D.: writing—review and editing. L.A. and M.S.: visualization. L.A.: supervision. R.L., C.I.-D., and L.A.: project administration. H.T. and C.I.-D.: funding acquisition. All authors have read and agreed to the published version of the manuscript.

This animal study was performed in strict accordance with the European Communities Council Directive of 22 September 2010 (2010/63/EU) and approved by the local authority on animal experiments (Berlin State Office for Health and Social Affairs, LaGeSo).

Conflicts of interest and sources of funding: This research was funded by the German Research Foundation in the scope of the collaborative research center "Matrix in Vision" (CRC 1340, projects B05 and C02, grant number 372486779). This study was also supported by scholarships from the Hertie Foundation to L.A. and from the Berlin Institute of Health (BIH) to R.L. C.I.-D. reports conference honoraria from Sanofi-Genzyme and research support from Sanofi-Genzyme, the Hertie Foundation, and the German Research Council (DFG). The funders had no role in the design of the study; in the collection, analyses, or interpretation of data; in the writing of the manuscript; or in the decision to publish the results. The remaining authors declare no conflicts of interest.

Correspondence to: Lina Anderhalten, MD, PhD, Experimental and Clinical Research Center (ECRC), Charité–Universitätsmedizin Berlin, Campus Buch, Lindenberger Weg 80, Berlin 13125, Germany. E-mail: lina-carlotta.anderhalten@charite.de.

Supplemental Digital Content is available for this article. Direct URL citations are provided in the HTML and PDF versions of this article on the journal's website, www.investigativeradiology.com.

ISSN: 1536-0210
DOI: 10.1097/RLI.0000000000001315

space and time.[4] In this context, contrast-enhanced magnetic resonance imaging (CE-MRI) plays a central role as gadolinium-based contrast agents (GBCAs) visualize blood-brain barrier (BBB) disruption as a key morphologic correlate of active inflammation in MS and allow discrimination between active, contrast-enhancing lesions and inactive, nonenhancing lesions.[5–7] Consequently, CE-MRI enables demonstration of dissemination in time already at the first examination.[4,5,7]

Despite their diagnostic utility, the in vivo safety of repeated intravenous administration of GBCAs has been the subject of continued debate.[8,9] While free gadolinium (Gd) ions (Gd^{3+}) are highly toxic, chelation by organic ligands improves GBCA solubility and in vivo kinetic stability,[10] which is higher for macrocyclic than for linear agents.[10–13] Accordingly, linear GBCAs partially dechelate in vivo post-injection,[13,14] resulting in Gd^{3+} release and retention in multiple organs, including the CNS.[15–21] Consequently, the Food and Drug Administration issued class warnings against linear GBCAs,[22] leading to their restricted use or discontinuation in many countries.[23] In contrast, macrocyclic GBCAs are generally assumed to be cleared from the body as intact chelates[21,24–28] and are currently the recommended contrast agents for CE-MRI, also in patients with MS.[4,7,29] Nevertheless, ongoing efforts focus on developing GBCAs with improved stability and relaxivity while reducing administered doses without compromising diagnostic performance.[30–32]

In MS, intracerebral Gd retention has been reported following repeated administration of both linear GBCAs[15,33–38] and macrocyclic GBCAs.[39,40] Although under normal conditions, there are no confirmed clinical consequences of intracerebral Gd retention,[41–44] preexisting neuroinflammation and chronic exposure to particularly linear agents may increase neurotoxic risks[45] and lead to alterations in cognitive function.[46,47] Accordingly, some MS studies reported lower verbal fluency[48,49] and information-processing speed[49] after linear GBCA administration. The concern of Gd retention, therefore, remains relevant in chronic inflammatory diseases, including MS, in which patients have historically been exposed to multiple CE-MRI examinations over prolonged periods.

In this context, repeated linear gadopentetate-dimeglumine (gadopentetate) administration in experimental autoimmune encephalomyelitis (EAE) in vivo led to sustained, inflammation-promoted cerebellar Gd retention persisting for weeks in mice,[27,50] whereas macrocyclic gadobutrol showed only transient, inflammation-associated accumulation followed by efficient clearance.[27] Mechanistically, electron paramagnetic resonance (EPR) spectroscopy provided evidence for Gd^{3+} release after gadopentetate administration in EAE mice in vivo, with subsequent binding to inorganic ligands and proximity to phosphorus-containing molecules in cerebellar tissue. In contrast, no Gd^{3+} release after gadobutrol administration was observed, consistent with preserved complex stability and subsequent elimination.[51] Furthermore, in organotypic hippocampal slice cultures, gadopentetate exposure impaired neuronal viability, particularly in an inflammatory milieu, whereas gadobutrol showed no cytotoxic effects at equivalent concentrations.[27]

Nevertheless, the effects of chronic GBCA exposure on living hippocampal tissue under inflammatory conditions remain insufficiently understood, especially at clinically relevant, sub-cytotoxic concentrations. Mitochondrial impairment has been implicated as a key mechanism of Gd-induced toxicity,[41] and neuronal mitochondrial dysfunction is recognized as an early and central feature of MS pathology,[52,53] closely linked to inflammation-driven oxidative stress and reactive oxygen species production.[53–56] Beyond overt cytotoxicity, subcytotoxic effects of retained Gd may contribute to subtle cognitive impairments, particularly after linear GBCA exposure. Given the critical role of the hippocampus in cognitive function and the strong association between hippocampal atrophy and cognitive impairment in MS,[3] this region is of particular interest for investigating GBCA-related mitochondrial toxicity.

Based on these considerations, we hypothesized that neuroinflammation contributes to increased cumulative Gd retention within the hippocampus and exacerbates GBCA-induced alterations in neuronal mitochondrial dynamics. Building on previously established mouse models of neuroinflammation and mitochondrial live imaging,[57–60] here, we investigated hippocampal Gd retention kinetics and spatial distribution patterns following repeated in vivo administration of linear gadopentetate and macrocyclic gadobutrol as representative GBCAs in EAE and healthy control (HC) mice using laser ablation inductively coupled plasma-time-of-flight mass spectrometry (LA-ICP-ToF-MS). Moreover, we examined the effects of exposure to both agents on neuronal mitochondrial morphology and motility under inflammatory and noninflammatory conditions ex vivo in chronic murine hippocampal slice cultures using a standardized, semi-automated analysis pipeline[58] alongside manual segmentation. The slice Gd content after ex vivo GBCA exposure was additionally quantified using ICP-MS.

MATERIALS AND METHODS

Ethics Statement and Animals

This study adhered to the European Communities Council Directive of September 22, 2010 (2010/63/EU) and received approval from the Berlin State Office for Health and Social Affairs (LaGeSo; approval-IDs: TCH0008/20, G106/19). Mitochondrial alterations were analyzed in hippocampal tissue from B6.Cg-Tg(Thy1-CFP/COX8A)S2Lich/J mice ("mitoCFP mice," own breading, Berlin Buch, Germany). These mice express cyan fluorescent protein (CFP) fused to human cytochrome c oxidase subunit 8A, driven by the Thy1 promoter gene.[61] This targeted CFP expression in neuronal mitochondria enables the visualization of mitochondrial motility and morphology using fluorescence microscopy.

Mouse Model of Experimental Autoimmune Encephalomyelitis and In Vivo Study Design

Experimental autoimmune encephalomyelitis (EAE) was actively induced in female SJL/J mice aged 9 to 10 weeks (Janvier Labs, France; n = 12) by subcutaneous immunization as previously reported.[27] The mice received 250 μg proteolipid protein peptide ($PLP_{139–151}$; purity 95%; Pepceuticals, Leicester, UK) and 800 μg *Mycobacterium tuberculosis* H37Ra (Difco, Franklin Lakes, NJ) in 100 μL complete Freund's adjuvant. In addition, on day 0 and day 2 post-immunization, 250 ng pertussis toxin (List, Biological Laboratories, Campbell, CA) was injected intraperitoneally. The EAE mice were monitored and scored daily for clinical deficiency.[27] Starting on days 12 to 13 post-immunization, when EAE mice showed maximal disability, EAE and HC mice (n = 12 per condition) received one intravenous injection via the tail vein daily of either the linear GBCA gadopentetate (Magnevist, Bayer, Germany; n = 12) or the macrocyclic GBCA gadobutrol (Gadovist, Bayer, Germany; n = 12) at 2.5 mmol/kg body weight over 4 consecutive days, followed by a 2-day break and 4 additional daily

injections, resulting in 4 experimental groups (EAE + gadopentetate, EAE + gadobutrol, HC + gadopentetate, HC + gadobutrol; n = 6 mice per group).[27]

Tissue Processing

Within each experimental group (n = 6), 2 mice were sacrificed at 1, 10, and 40 days after the final GBCA injection (post-final injection, p.f.i.) and transcardially perfused with 0.1 M PBS. Brains were isolated, fixed in 4% paraformaldehyde (PFA) and 30% sucrose, embedded, and frozen (−80 °C). For LA-ICP-ToF-MS of midbrain sections (n = 2/experimental group and timepoint of sacrifice), brains were cut coronally, separating the forebrain, midbrain, and cerebellum. Frozen midbrains were then cut in the coronal plane into 10-µm-thick cryosections and stored at −80 °C until ablation.

LA-ICP-ToF-MS Analysis of Hippocampal Gd Concentrations After In Vivo GBCA Application

Laser ablation of 10-µm-thick cryosections of the midbrain (1, 10, or 40 d p.f.i.), containing the hippocampus, was performed using a NWRimage laser ablation system (266 nm, Elemental Scientific Lasers, Bozeman, MT) equipped with a low-dispersion ablation cup in a TwoVol3 ablation chamber attached to an ICP-ToF-MS (Model 2R, Tofwerk AG, Thun, Switzerland) using a 0.762 mm ID PEEK tubing, a Dual Concentric Injector (DCI2) and combined helium (He) and argon (Ar) flow.[62] Instrumental settings are summarized in Table SDC_1 in the Supplemental Digital Content 1, https://links.lww.com/RLI/B130. The laser ablation system was controlled by the ActiveView2 software (Elemental Scientific Lasers, Bozeman, MT). A square laser beam of 10 µm×10 µm was used, and samples were scanned with a repetition rate of 100 Hz and a fluence of 9 J/cm^2. Data acquisition was triggered for every ablation position using the laser ablation workflow of TofPilot (Tofwerk AG, Thun, Switzerland), acquiring the entire image as a single Hierarchical Data Format (HDF5) file. Data post-processing of the acquired images and calibration materials was conducted in the Iolite v4 software (Elemental Scientific Lasers, Bozeman, MT). The HDF5 files were loaded in Iolite v4 software, and the data were reduced using the "3D Trace Elements" data reduction scheme (3D-TE-DRS).[63,64] Further details of the analytical routine, including calibration procedures,[65] are described in the Supplemental Digital Content 1, https://links.lww.com/RLI/B130 and in Schannor et al.[66]

For the quantification of retained Gd concentrations (in µg/g) in the whole midbrain slice (mean), hippocampus, and dentate gyrus (DG), manual regions of interest (ROIs) were defined on the calibrated LA-ICP-ToF-MS copper (Cu) images. Copper distribution images provided a clear visualization of brain anatomy, enabling accurate delineation of the hippocampi and DGs from the surrounding midbrain tissue. These ROI masks were subsequently applied to the corresponding Gd maps to determine Gd concentrations. Left and right hippocampi and DGs were quantified separately, and the values were then averaged. Image analysis was performed in an independent and randomized manner using ImageJ software.[67]

Generation of Organotypic Hippocampal Slice Cultures

MitoCFP mouse pups aged 7 to 10 days (n = 12) were sacrificed by decapitation, and slice cultures were generated as previously described.[58] In brief, the sculp was removed and the skull placed in chilled cutting medium [1x MEM (Gibco, Thermo Fisher Scientific Inc., Waltham, MA) with 1% L-Glutamine (Merck, Darmstadt, Germany)]. The skull was opened under a sterile bench, and both hippocampi were isolated and cut coronally into 350 µm-thick slices using a McIlwain Tissue Chopper (Mickle Laboratory Engineering Co Ltd, Guildford, Surrey, UK). Slices were examined under a basic light microscope before the membrane transfer (PICM0RG50, Millicell cell culture inserts, 0.4 µm, Merck, Darmstadt, Germany) to identify histologically intact exemplars. The entire process of slice preparation never exceeded a time limit of 30 minutes. Chronic slice cultures were preincubated natively for 2 weeks at 37 °C and 5% CO_2, while the culture medium was exchanged every second day.[58]

Experimental Ex Vivo Setup

To assess GBCA effects on mitochondria under inflammatory and noninflammatory conditions, on day 13, hippocampal slices were exposed to different concentrations of gadopentetate or gadobutrol in the presence or absence of TNF-alpha (TNFα) at 50 ng/mL for 48 hours at 37 °C and 5% CO_2, as depicted in Figure 1. The slices were divided into 4 treatment groups: (1) gadopentetate without TNFα, (2) gadopentetate with TNFα at 50 ng/mL, (3) gadobutrol without TNFα, and (4) gadobutrol with TNFα at 50 ng/mL. For each treatment group, GBCAs were applied at concentrations of 0.1, 1, 10, and 50 mM, respectively.[27]

These concentrations were selected to cover a broad exposure range from sub-cytotoxic to cytotoxic conditions based on our previous studies.[27,51] As only a fraction of the applied GBCA is expected to be retained within the slice tissue after 48 hours of incubation,[51] resulting intratissue Gd concentrations are substantially lower than the applied concentrations. Accordingly, the lower (0.1, 1 mM) and intermediate (10 mM) exposure conditions were selected to yield intratissue Gd concentrations in the micromolar to submicromolar range, which are biologically relevant and within the order of magnitude reported or extrapolated following clinically relevant GBCA administration in experimental animal models at human-equivalent doses and in human brain tissue after clinical GBCA exposure,[68–71] whereas 50 mM served as a high-dose condition approaching the cytotoxic threshold in this experimental model.[27]

To further establish corresponding negative controls, slices were incubated in the absence of GBCAs, with or without TNFα, for 48 hours. For optimal penetration of substances into the living tissue, 100 µL medium was applied on top of the hippocampal slices on each culture membrane. Three independent replicates per condition were conducted using the same experimental setup with 6 to 7 hippocampal slices per membrane. To control for different incubation periods, the time of substance exposure was aligned with the imaging time point 2 days later.

For ICP-MS assessment of Gd content after GBCA exposure (see the ICP-MS Quantification of Slice Gadolinium Content After Ex Vivo Administration section), chronic slices were treated with gadopentetate or gadobutrol ± TNFα at 50 ng/mL for 48 hours ex vivo as done for analysis of mitochondrial dynamics (Fig. 1). In this case, however, only GBCA concentrations of 10 and 50 mM were applied, as the strongest mitochondrial and cytotoxic[27] effects were expected at high to intermediate concentrations. Three replicates per condition were conducted, with 6 to 7 slices per membrane.

Live Imaging and Semi-Automated Analysis of Mitochondrial Motility and Morphology

After treatment termination on day 15, membranes with hippocampal slices were excised and transferred to glass-bottom plates (CellVis, P06-1.5H-N, Mountain View, CA) with imaging

medium (FluoroBrite DMEM, 1% HEPES, 1% Pen/Strep) for live imaging.[58] Imaging of fluorescent mitochondria was performed according to a previously established protocol using a Nikon Spinning Disk Confocal CSU-X with chamber conditions set to 37 °C and 5% CO_2.[58] In brief, time-lapse sequences of the dentate gyrus (DG) were acquired at 40× magnification with standard laser and exposure settings, restricted to 45 minutes to preserve slice viability (Fig. 1). Time lapses were acquired over 2-minute intervals, with frames captured every 4 seconds (31 frames/sequence). Per treatment condition, 4 slices with intact DGs were imaged, with 3 random ROIs per slice, yielding 12 time-lapse sequences per condition.

An established, in-house developed macro[58] for ImageJ software (version 2.14.0) was used to assess mitochondrial morphology and motility in acquired image sequences in a semi-automated manner. Technical details of this image analysis have been described elsewhere[58] and are additionally summarized in Figure SDC_2 (Supplemental Digital Content 3, https://links.lww.com/RLI/B140). In brief, mitochondrial motility was analyzed using StackReg[72,73] (http://bigwww.epfl.ch/thevenaz/stackreg/) and TrackMate (version 7.11.1).[73,74] Once, the semi-automated image analysis was completed, relevant datasets concerning mitochondrial speed and displacement, mitochondrial area, mitochondrial length, and aspect ratio [shape from perfect circularity[1] to elongation (>1–∞)] were extracted. Importantly, mitochondrial displacement reflects the full distance mitochondria traveled along their path, not just the straight-line distance between start and end points. Finally, the fraction of motile mitochondria was calculated from morphology and motility measures for each of the 12 selected ROIs.

An additional manual analysis using ImageJ software was performed in a randomized and blinded manner (2 independent rounds for the morphology analysis, and 1 round for motility analysis) to validate the performance of our semi-automated analysis (for manual results see Tables SDC_5 and SDC_6, Supplemental Digital Content 4, https://links.lww.com/RLI/B141).

ICP-MS Quantification of Slice Gadolinium Content After Ex Vivo Administration

Chronic hippocampal slices were assessed for Gd content after 48 hours of incubation with gadopentetate or gadobutrol at 10 or 50 mM ± TNFα, respectively (see the Experimental Ex Vivo Setup section). Untreated and TNFα-treated slices served as negative controls. After treatment, membranes were excised and dipped into fresh culture medium for the removal of superficial GBCA-containing culture medium. Subsequently, they were fixed in 4% PFA for 1 hour to enable slice removal from the membranes of cell culture inserts. No mitochondrial imaging or any further washing steps were conducted on these slices to avoid additional washout of potentially intact agents. 18 to 21 isolated slices (n = 6 to 7 per replicate membrane) were pooled per culture condition, yielding 2.52 ± 0.19 mg each, and further digested overnight in 0.5 mL concentrated nitric acid (sub-boiled) and 25 µL of hydrogen peroxide (30%, ultrapure). For complete digestion, samples were heated to 95 °C using a thermomixer (Eppendorf, Hamburg, Germany) for 2 hours and subsequently filtered and diluted to a volume of 15 mL in deionized water (MilliQ system, Millipore, Eschborn, Germany). Measurements were acquired using an Element 2 ICP-sector-field-MS (Thermo Fisher Scientific, Bremen, Germany). Instrumental parameters of the ICP-MS system for Gd detection ex vivo, as well as information on calibration, are detailed in Table SDC_7 (Supplemental Digital Content 5, https://links.lww.com/RLI/B142).

Statistics

The data were statistically analyzed using GraphPad Prism 8.4.3 (GraphPad, CA). LA-ICP-ToF-MS data from the in vivo trial (n = 2/experimental group and timepoint) and ICP-MS data from the ex vivo trial (n = 3 replicates pooled for analysis/condition) were expressed descriptively as geometric means ± standard deviations (SD). For ex vivo imaging data, comparisons between more than 2 groups were performed using the Kruskal-Wallis test followed by Dunn's post hoc test for multiple rank comparisons. Two-group comparisons additionally were performed for each condition within the same GBCA treatment group (+TNFα vs. −TNFα) using the Mann-Whitney *U* test. This approach was applied across all experimental conditions per GBCA without Bonferroni correction for multiple comparisons. The aim here was to uncover any stochastic dominance and thus any effect of neuroinflammation. *P* values should therefore be evaluated rather descriptively (with * implying $P < 0.05$, ** implying $P < 0.01$, *** implying $P < 0.001$, and **** implying $P < 0.0001$).

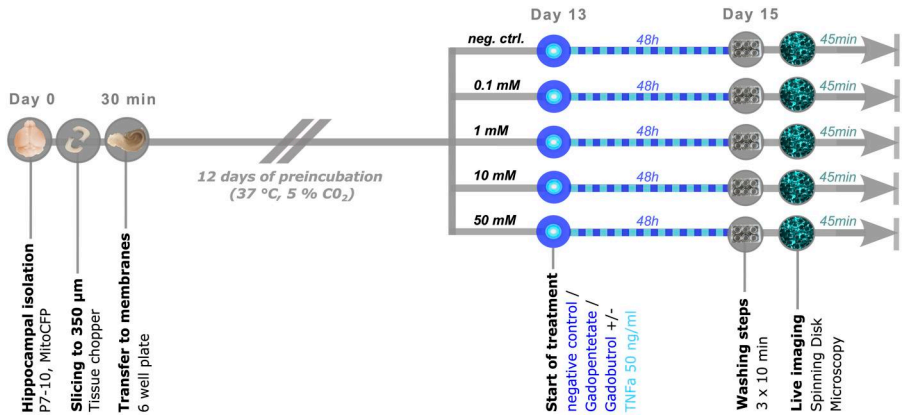

FIGURE 1. Illustration of the ex vivo study design. On day 0, MitoCFP pups were sacrificed, and hippocampal sections were generated and transferred to culture membranes. After 12 days of culture stabilization, the slices were divided into 4 GBCA treatment groups (gadopentetate or gadobutrol ± TNFα). Within each group, slices were exposed to 0.1, 1, 10 or 50 mM GBCA for 48 hours. In addition, inflammatory (TNFα only) and noninflammatory (completely untreated) negative controls were included. On day 15, live imaging of fluorescent neuronal mitochondria was performed for 45 minutes per culture condition.

RESULTS

LA-ICP-ToF-MS Reveals Inflammation-Driven Hippocampal Gadolinium Retention

Hippocampal Gd retention was quantified by LA-ICP-ToF-MS in representative 10-µm-thick cryosections of the midbrain on days 1, 10, and 40 p.f.i. of gadopentetate or gadobutrol (n = 2/experimental group and timepoint). As shown in Figure 2A, gadopentetate-treated EAE mice exhibited Gd retention within the hippocampus and across multiple deep gray matter and cortical regions, including the caudoputamen, globus pallidus, dorsal thalamus, and isocortex, particularly the retrosplenial and somatomotor areas. Specifically, within the cortex, globus pallidus and caudoputamen, Gd was retained in a scattered pattern with local hotspots (Fig. SDC_1, Supplemental Digital Content 1, https://links.lww.com/RLI/B130). HC mice treated with gadopentetate showed similar retention patterns; however, cortical Gd signals were less pronounced by day 40 p.f.i. In contrast, gadobutrol administration in both HC and EAE mice produced a more diffuse Gd signal distribution, predominantly within periventricular areas. This periventricular signal was more prominent in EAE mice on day 1 and largely resolved by day 40 p.f.i. in both groups.

Across the 3 ROIs (whole midbrain slice, hippocampus, and DG) from which kinetics of mean Gd concentrations were derived (Fig. 2B), gadopentetate-treated EAE mice exhibited 2- to 4-fold higher Gd concentrations than HC mice at day 1 p.f.i. (EAE vs. HC, DG: 3.114 ± 0.431 µg/g vs. 0.797 ± 0.125 µg/g) and retained measurable levels at day 40 p.f.i. (EAE vs. HC, DG: 0.494 ± 0.167 µg/g vs. 0.246 ± 0.003 µg/g). Gadobutrol-treated mice showed markedly lower absolute concentrations with a 2- to 3-fold EAE/HC difference at day 1 p.f.i. (EAE vs. HC, DG: 1.287 ± 1.555 µg/g vs. 0.650 ± 0.460 µg/g), but near-complete clearance by day 40 p.f.i. (0.003 µg/g in both hippocampus and DG). Gadolinium concentrations detected within the respective ROIs are fully detailed in Table SDC_2 (Supplemental Digital Content 1, https://links.lww.com/RLI/B130).

In addition, elemental distributions of zinc (Zn), copper (Cu), calcium (Ca), phosphorus (P), sulfur (S), manganese (Mn), and iron (Fe) were assessed. Following injection of both GBCAs, no temporal changes were detected for any of these endogenous elements, indicating that their distribution within the chosen ROIs remained stable over time regardless of the GBCA administered. As indicated in the Supplemental Figure SDC_1 (Supplemental Digital Content 1, https://links.lww.com/RLI/B130), the hippocampus showed high Zn levels, particularly in the molecular layers corresponding to fiber-rich regions. Notably, after gadopentetate administration, Gd co-localized with Fe predominantly within neuron-rich pyramidal cell layers of CA1-CA3 within the hippocampus. In addition to the hippocampus, Fe levels were high and overlapped with Gd retention in the basal ganglia, particularly the globus pallidus, while Cu displayed a distinct distribution pattern, with strong enrichment in periventricular areas Figure SDC_1 (Supplemental Digital Content 1, https://links.lww.com/RLI/B130).

Both Gadopentetate and Gadobutrol Alter Mitochondrial Dynamics Ex Vivo

Using chronic hippocampal slice cultures, we assessed the effect of gadopentetate and gadobutrol at 0.1, 1, 10, and 50 mM for 48 hours, respectively, on neuronal mitochondria ex vivo within the DG region under inflammatory (+TNFα) and noninflammatory (−TNFα) conditions. Video material of time-lapse sequences of neuronal mitochondria in slices treated with 10

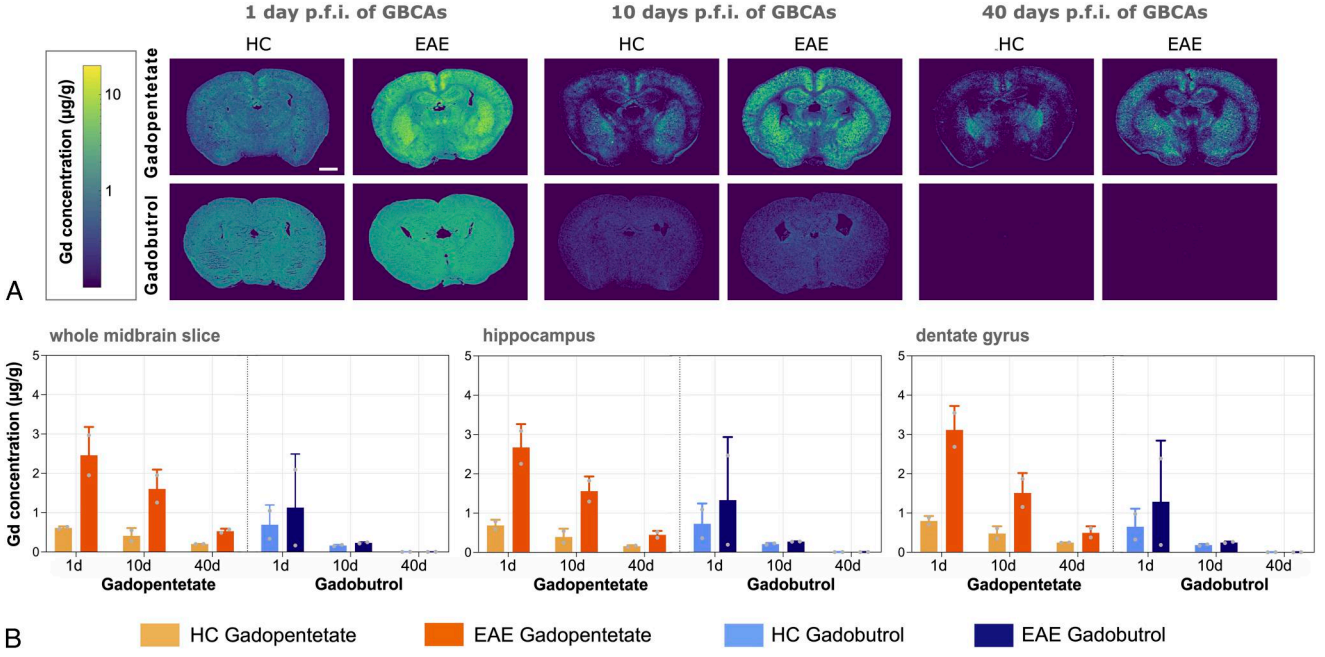

FIGURE 2. Analysis of spatiotemporal Gd retention patterns in murine midbrain sections using LA-ICP-ToF-MS following the in vivo administration of gadopentetate or gadobutrol at a cumulative dose of 20 mmol/kg BW. (A) Analysis of Gd distribution in midbrain section 1, 10, and 40 days p.f.i. of GBCAs in EAE and HC mice. Scale bar: 1 mm. (B) Quantification of Gd concentrations (in µg/g) within the whole midbrain slice (on the left), the hippocampus (middle), and the DG (on the right) of EAE and HC mice (n = 2/experimental group). Due to the small sample size, only descriptive statistics are reported (mean ± SD).

or 50 mM gadopentetate or gadobutrol ± TNFα, as well as negative controls ± TNFα, is provided in the Supplemental Digital Content 2, Video 1, Video 2, Video 3, Video 4, Video 5, Video 6, Video 7, Video 8, Video 9, Video 10.

First, mitochondrial morphology and motility were qualitatively evaluated in live imaging sequences by visual inspection (Fig. 3). In negative control slices (± TNFα, no GBCA) and slices treated with both GBCAs at 0.1 or 1 mM (± TNFα), respectively, mitochondria generally appeared elongated and displayed directed movement along neuronal axons.

As shown in Figures 3A and B, in slices treated with gadopentetate at 10 or 50 mM under inflammatory and noninflammatory conditions, mitochondria appeared shorter. In slices treated with gadopentetate at 10 mM under inflammatory conditions, a subset of mitochondria appeared enlarged or clustered together. At 50 mM, mitochondria additionally exhibited a circular shape and their movements became uncoordinated and undirected (ie, back and forth in place), particularly under inflammatory conditions.

In contrast, in slices treated with gadobutrol under noninflammatory conditions, mitochondria remained elongated and motile at concentrations up to 10 mM. Only at 50 mM, they appeared shorter (Fig. 3A) with reduced displacement, although directional movement along axons was still visible. Under inflammatory conditions, gadobutrol at 10 mM had little effect on morphology or motility. At 50 mM, however, mitochondria appeared shorter (Figs. 3A, B) and moved less directionally, frequently oscillating back and forth in place.

Gadopentetate Exposure Alters Neuronal Mitochondrial Morphology Already at Low Doses and Is Modulated by Inflammation

Using a previously established semi-automated image analysis approach,[58] we quantified alterations in mitochondrial area, length, and aspect ratio (ie, circularity) in chronic hippocampal slices after gadopentetate exposure ex vivo.

Under noninflammatory conditions, mitochondria became smaller and shorter ($P < 0.0001$, respectively) across all tested concentrations of gadopentetate compared with negative controls (Figs. 4A, B). The strongest reduction in mitochondrial length was observed at 50 mM of gadopentetate (negative control vs. 50 mM gadopentetate; 1.580 ± 0.441 µm vs. 1.402 ± 0.481 µm, $P < 0.0001$), accompanied by a significant reduction in area (untreated control vs. 50 mM gadopentetate; 0.896 ± 0.460 µm^2 vs. 0.726 ± 0.513 µm^2, $P < 0.0001$).

Under inflammatory conditions (Figs. 4C, D), mitochondria were significantly smaller and shorter after 50 mM gadopentetate exposure compared with respective negative controls (negative control+ TNFα vs. 50 mM gadopentetate+TNFα; area: 0.790 ± 0.476 µm^2 vs. 0.669 ± 0.448 µm^2, length: 1.475 ± 0.449 µm vs. 1.376 ± 0.442 µm, both $P < 0.0001$), representing the strongest reduction in area and length observed

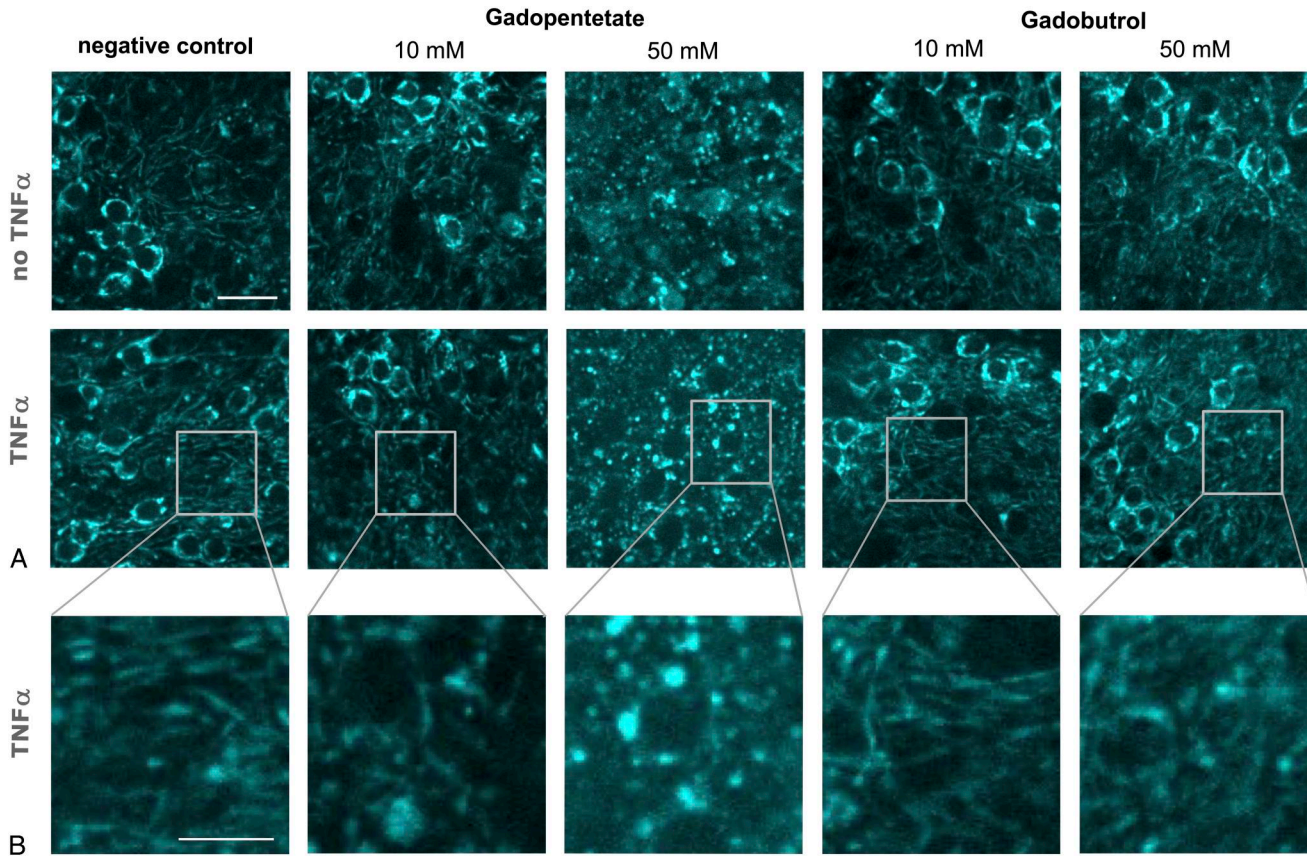

FIGURE 3. Confocal microscopy assessment of mitochondrial morphology upon GBCA treatment ± TNFα, respectively. (A) Representative confocal microscopy images (first image of a sequence containing 31) at ×40 magnification showing fluorescent mitochondria in chronic slices treated with gadopentetate or gadobutrol at 10 and 50 mM ± TNFα compared with the respective negative controls. Scale bar 20 µm. (B) Illustration of enlarged image sections for visualization of mitochondrial morphology under inflammatory conditions. Scale bar 10 µm.

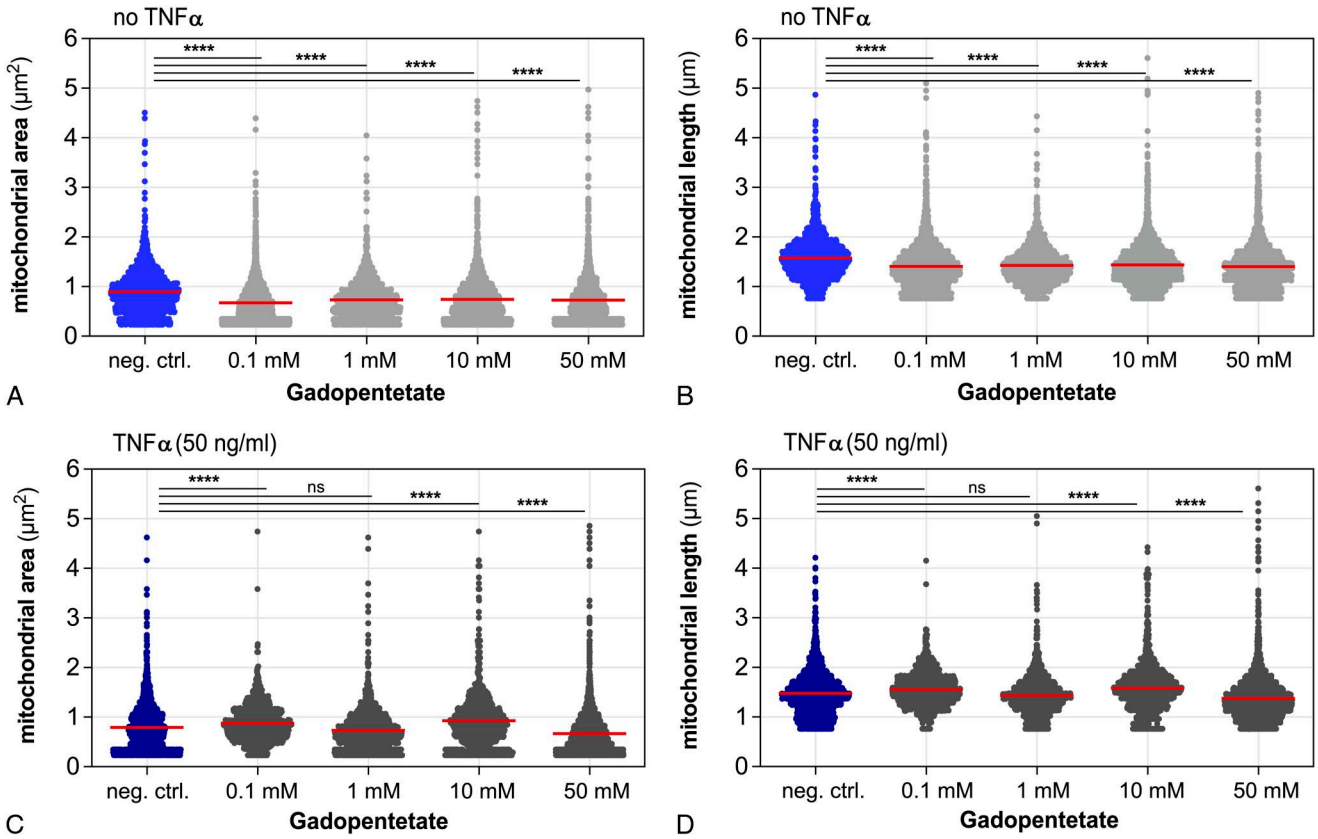

FIGURE 4. Semi-automated analysis of mitochondrial area and length after 48 hours of incubation with gadopentetate, comparing negative controls (±TNFα) to GBCA conditions (±TNAα), respectively. Red lines indicate the mean values. Results for 2 treatment groups are shown: (1) negative control (n = 10,996) versus gadopentetate at 0.1 (n = 17,580), 1 (n = 13,431), 10 (n = 15,374), 50 mM (n = 14,945) without TNFα; (2) negative control (n = 10,585) versus gadopentetate at 0.1 (n = 9302), 1 (n = 12,835), 10 (n = 8953), 50 mM (n = 21,051) with TNFα at 50 ng/mL. Kruskal-Wallis test, followed by Dunn's post hoc test. ****$P < 0.0001$.

across all experiments. In contrast, mitochondria under inflammatory conditions were larger and longer at 0.1 and at 10 mM of gadopentetate (area: 0.929 ± 0.567 µm², length: 1.582 ± 0.506 µm, both $P < 0.0001$ compared with controls). At 10 mM under inflammatory conditions, the semi-automated analysis detected the strongest decrease in aspect ratio ($P < 0.05$), consistent with the qualitatively observed increase in rounded and swollen or clustered mitochondria (see the Both Gadopentetate and Gadobutrol Alter Mitochondrial Dynamics Ex Vivo section; also see Tables SDC_3 and SDC_4, Supplemental Digital Content 3, https://links.lww.com/RLI/B140, for full results).

Direct comparison between slices cultured under inflammatory versus noninflammatory conditions confirmed that TNFα-treated negative controls already showed smaller mitochondrial area and length compared with untreated negative controls (in blue, both $P < 0.0001$, uncorrected Mann-Whitney tests; see supplemental Table SDC_3, Supplemental Digital Content 3, https://links.lww.com/RLI/B140). At 0.1 and 10 mM gadopentetate, the reductions in area and length observed in the control conditions were partly attenuated under inflammatory conditions, while at 50 mM, inflammation further exacerbated the reduction in area ($P < 0.001$), with a similar trend for length.

Together, these results show that gadopentetate induces pronounced effects in neuronal mitochondrial morphology already at low concentrations, which seem to be modulated under inflammatory conditions. While gadopentetate alone consistently reduced mitochondrial size and length, its effects in the presence of TNFα were dose-dependent: low to intermediate concentrations partially attenuated TNFα-induced mitochondrial contraction, whereas the highest concentration (50 mM) exacerbated this effect.

Gadobutrol Reduces Neuronal Mitochondrial Size and Length Ex Vivo With Enhanced Effects Under Inflammation

Under noninflammatory conditions, gadobutrol exposure led to significantly smaller mitochondria at nearly all tested concentrations compared with negative controls ($P < 0.0001$, respectively; Fig. 5A). The only exception was the 10 mM dose, which only showed a trend toward area reduction. As shown in Figure 5B, mitochondrial length was also significantly decreased at all concentrations, particularly with 50 mM gadobutrol (negative control vs. 50 mM gadobutrol; 1.580 ± 0.441 µm vs. 1.446 ± 0.357 µm, $P < 0.0001$).

Under inflammatory conditions, gadobutrol similarly reduced mitochondrial area and length at all concentrations (Figs. 5C, D), which was significant for most conditions ($P < 0.0001$, respectively, except at 1 and 10 mM; Table SDC_3, Supplemental Digital Content 3, https://links.lww.com/RLI/B140). At 50 mM, gadobutrol produced the strongest

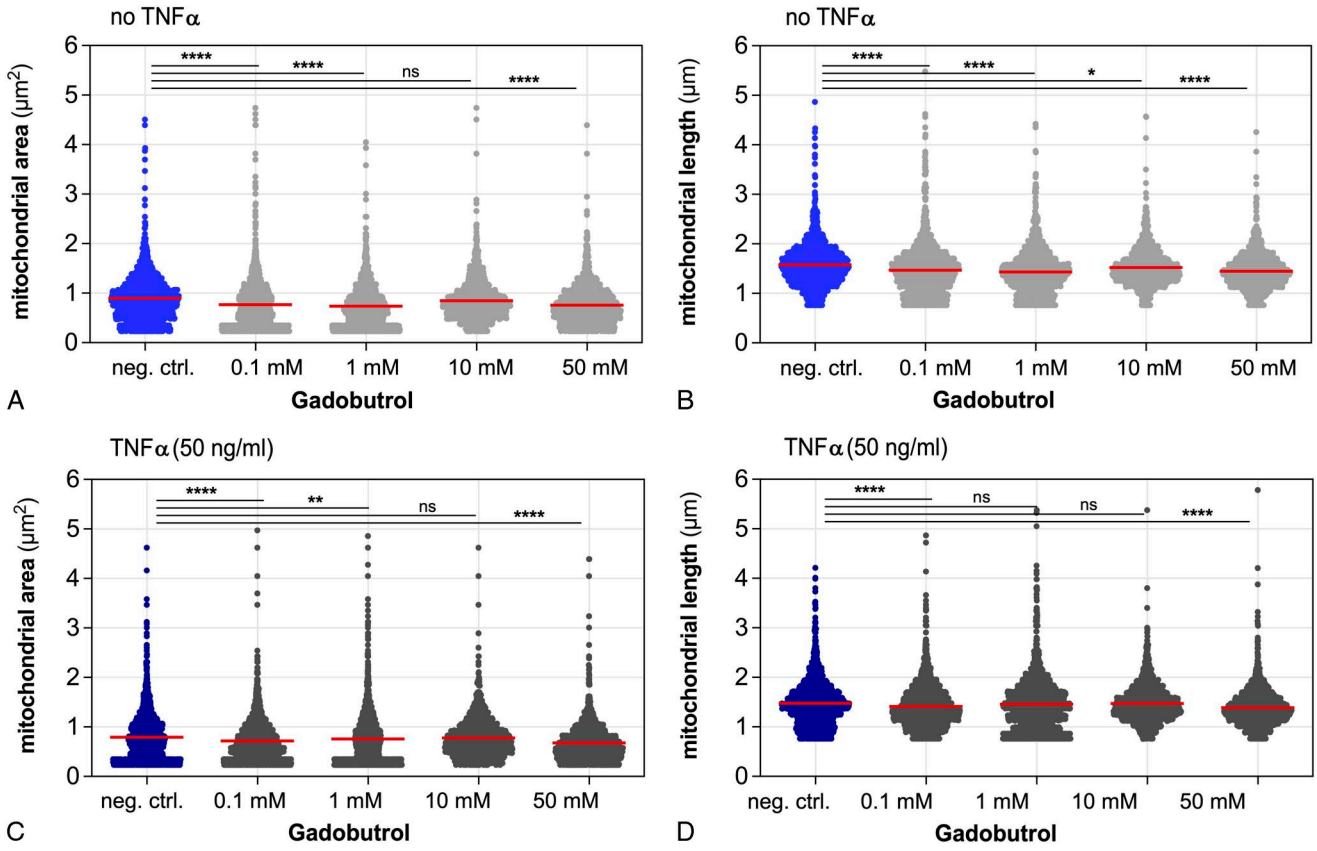

FIGURE 5. Semi-automated analysis results for mitochondrial area and length after 48 hours of incubation with gadobutrol, comparing negative controls (± TNFα) to GBCA conditions (± TNAα), respectively, using the Kruskal-Wallis test, followed by Dunn's post hoc test. Red lines indicate the mean values. Results for 2 treatment groups are shown: (1) negative control (n = 10,996) versus gadobutrol at 0.1 (n = 13,254), 1 (n = 11,184), 10 (n = 11,584), 50 mM (n = 11,905) without TNFα, and (2) negative control (n = 10,585) versus gadobutrol at 0.1 (n = 14,200), 1 (n = 12,247), 10 (n = 11,234), 50 mM (n = 13,334) with TNFα at 50 ng/mL. *$P < 0.05$, **$P < 0.01$, ****$P < 0.0001$.

reduction in both parameters compared with respective controls (negative control + TNFα vs. 50 mM gadobutrol + TNFα; area: 0.790 ± 0.476 µm² vs. 0.676 ± 0.366 µm², length: 1.475 ± 0.449 µm vs. 1.385 ± 0.343 µm, both $P < 0.0001$), paralleling the effects observed with gadopentetate, albeit to a slightly lower extent.

Direct comparison of inflammatory versus noninflammatory conditions (uncorrected Mann-Whitney tests; Table SDC_3, Supplemental Digital Content 3, https://links.lww.com/RLI/B140) showed that TNFα treatment alone significantly reduced mitochondrial area and length (both $P < 0.0001$). Inflammation accentuated gadobutrol-induced effects at all tested concentrations, particularly at 10 and 50 mM.

Thus, gadobutrol exposure induced mitochondrial changes comparable to gadopentetate under noninflammatory conditions, but diverged in the presence of TNFα, causing further reductions in mitochondrial size and length at all tested concentrations.

Gadopentetate Exposure Induces Concentration- and Inflammation-Dependent Alterations in Neuronal Mitochondrial Motility Ex Vivo

Our semi-automated assessment of mitochondrial motility revealed that gadopentetate under noninflammatory conditions altered mitochondrial speed in a concentration-dependent manner (Fig. 6A). Although all gadopentetate conditions showed a trend toward increased mitochondrial speed, only the effects at 1 mM ($P < 0.01$) and at 10 mM reached statistical significance compared with negative controls (negative control vs. 10 mM gadopentetate; 0.182 ± 0.125 µm/s vs. 0.202 ± 0.155 µm/s, $P < 0.0001$). By contrast, at 50 mM, mitochondrial speed was markedly reduced (speed: 0.166 ± 0.127 µm/s, $P < 0.0001$ compared with negative control).

However, in the slices cultured with TNFα, incubation with 50 mM gadopentetate increased mitochondrial speed compared with the respective negative control (negative control+TNFα vs. 50 mM gadopentetate +TNFα; 0.177 ± 0.124 µm/s vs. 0.211 ± 0.127 µm/s, $P < 0.0001$). Lower concentrations induced only a trend toward faster movement under inflammatory conditions (Fig. 6C; Table SDC_4, Supplemental Digital Content 3, https://links.lww.com/RLI/B140).

Generally, significant differences in track displacement between GBCA-treated slices and negative controls were observed under both conditions (Figs. 6B, D). The fraction of motile mitochondria was not significantly altered overall; however, gadopentetate exposure at 50 mM generally resulted in the lowest fractions detected (Table SDC_4, Supplemental Digital Content 3, https://links.lww.com/RLI/B140).

Comparing slices under inflammatory vs. noninflammatory conditions, TNFα alone had no relevant effect on mitochondrial speed or displacement in the absence of GBCA exposure. Under

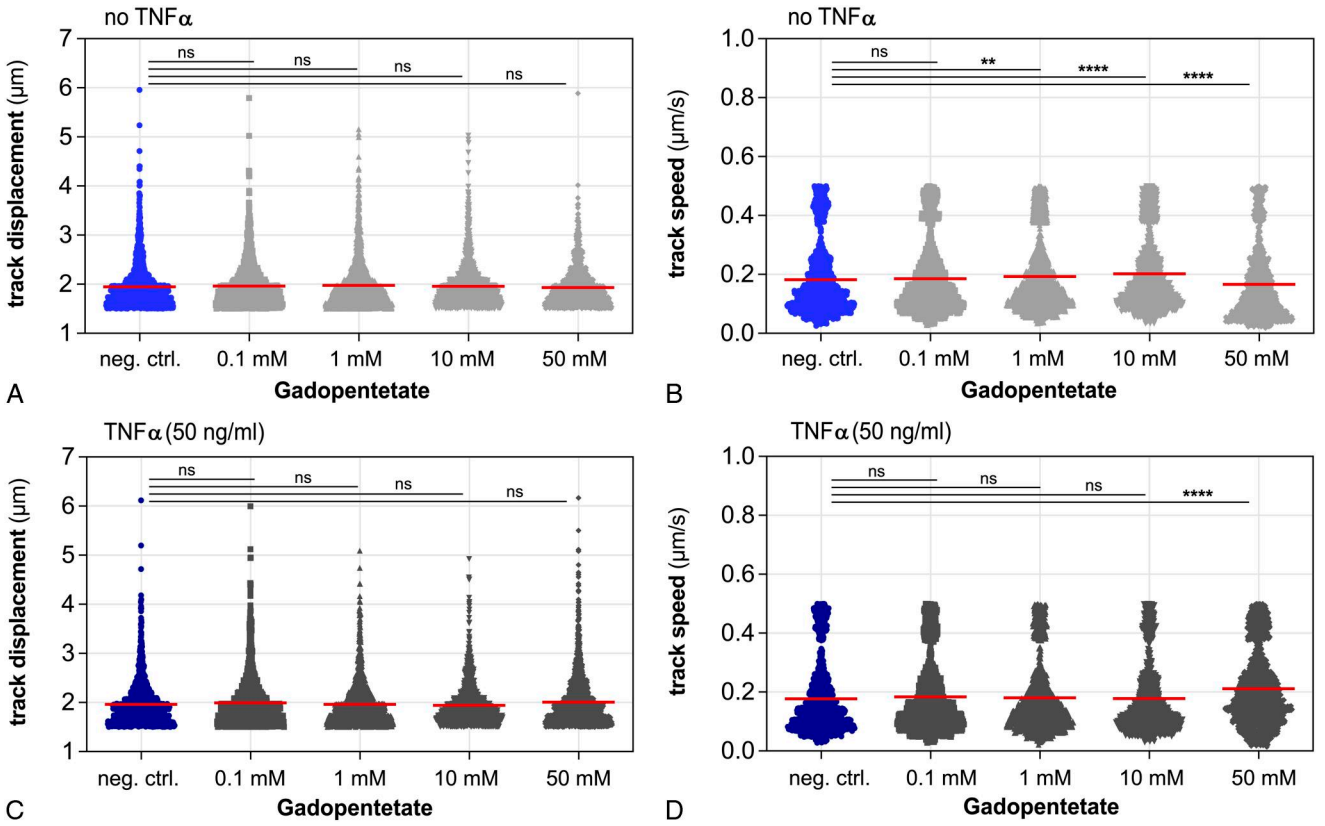

FIGURE 6. Semi-automated analysis of mitochondrial track speed and displacement after 48 hours of incubation with gadopentetate, comparing negative controls ± TNFα to GBCA conditions ± TNFα, respectively, using the Kruskal-Wallis test, followed by Dunn's post hoc test. Red lines indicate the mean values. Results for 4 treatment groups are shown: (1) negative control (n = 1419) versus gadopentetate at 0.1 (n = 1732), 1 (n = 1842), 10 (n = 1442), 50 mM (n = 1058) without TNFα; (2) negative control (n = 1282) versus gadopentetate at 0.1 (n = 1817), 1 (n = 1361), 10 (n = 1207), 50 mM (n = 1701) with TNFα at 50 ng/mL. $^{**}P < 0.01$, $^{****}P < 0.0001$.

gadopentetate treatment, however, inflammation appeared to mitigate gadopentetate-induced increases in track speed at concentrations of 1 and 10 mM, resulting in reduced track speed compared with non-inflammatory conditions (1 mM: $P < 0.001$; 10 mM: $P < 0.0001$). At 50 mM, this pattern reversed, with inflammation markedly enhancing mitochondrial speed ($P < 0.0001$) and displacement ($P < 0.01$), producing the strongest motility changes observed across all conditions. All single values, including fractions of motile mitochondria, are detailed in Table SDC_4 (Supplemental Digital Content 3, https://links.lww.com/RLI/B140).

Thus, gadopentetate alters neuronal mitochondrial motility ex vivo in an inflammation- and concentration-dependent manner. While gadopentetate generally increased mitochondrial speed at low to intermediate concentrations under non-inflammatory conditions, inflammation attenuated these effects and markedly enhanced motility at high concentrations.

Gadobutrol Exposure Enhances Mitochondrial Motility Ex Vivo Under Inflammatory and Noninflammatory Conditions

Although gadobutrol showed a tendency to increase mitochondrial speed at all concentrations in control slices (Fig. 7A), only effects at 0.1 mM ($P < 0.001$) and 50 mM were significant compared with negative controls, with the highest track speed detected at 50 mM (negative control vs. 50 mM gadobutrol; 0.182 ± 0.125 µm/s vs. 0.196 ± 0.463 µm/s, $P < 0.01$).

Under inflammatory conditions, very similar patterns were observed (Fig. 7C), with significantly faster mitochondria at all gadobutrol concentrations tested ($P < 0.05$ to $P < 0.0001$). Notably, at 50 mM in TNFα-treated slices, track speed reached its maximum out of all gadobutrol-treated conditions (negative control + TNFα vs. 50 mM gadobutrol + TNFα; 0.177 ± 0.124 µm/s vs. 0.210 ± 0.126 µm/s, $P < 0.0001$) and was comparable to that induced by gadopentetate at the same concentration.

Comparison of inflammatory versus noninflammatory conditions revealed that TNFα significantly promoted mitochondrial speed at 1 ($P < 0.05$) and 50 mM ($P < 0.0001$) of gadobutrol (Supplemental Table SDC_4, https://links.lww.com/RLI/B140). In addition, in TNFα-treated slices, mitochondria moved longer distances and the fraction of motile mitochondria increased compared with the noninflammatory setting after gadobutrol treatment at 50 mM (both $P < 0.01$).

Thus, gadobutrol increases neuronal mitochondrial motility in a concentration-dependent manner ex vivo, with inflammation amplifying mitochondrial speed, displacement, and the fraction of motile mitochondria, particularly at high concentrations.

Ex Vivo, Manual Mitochondrial Segmentation and Tracking Largely Confirm GBCA-induced Changes in Mitochondrial Dynamics

To validate the results of the quantitative semi-automated analysis, we additionally performed blinded manual mitochondrial

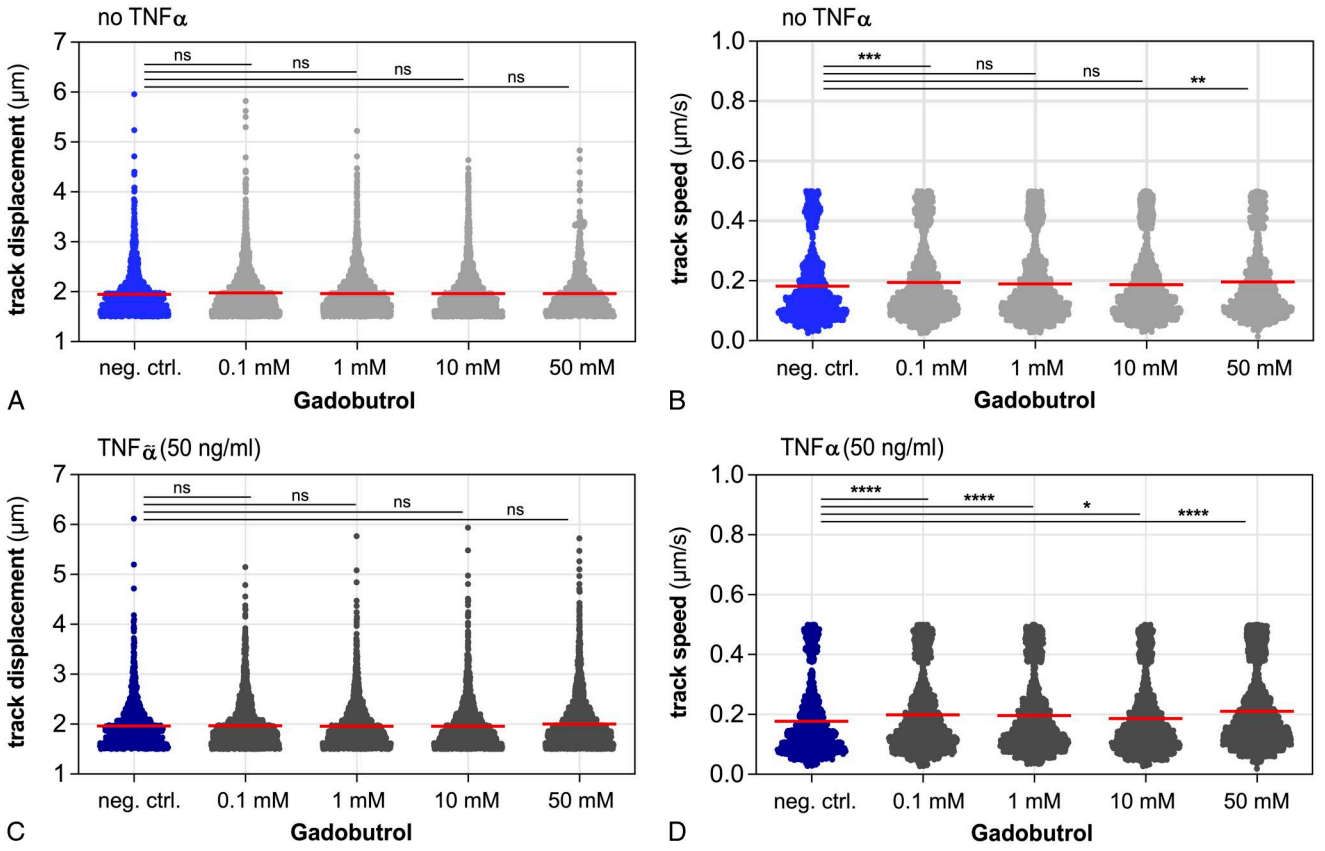

FIGURE 7. Semi-automated analysis of mitochondrial track speed and displacement after 48 hours of incubation with gadobutrol, comparing negative controls ± TNFα to GBCA conditions ± TNAα, respectively, using the Kruskal-Wallis test, followed by Dunn's post hoc test. Red lines indicate the mean values. Results for 2 treatment groups are shown: (3) negative control (n = 1419) versus gadobutrol at 0.1 (n = 2128), 1 (n = 2116), 10 (n = 2154), 50 mM (n = 1147) without TNFα, and (4) negative control (n = 1282) versus gadobutrol at 0.1 (n = 1909), 1 (n = 1893), 10 (n = 2137), 50 mM (n = 3001) with TNFα at 50 ng/mL. *$P < 0.05$, **$P < 0.01$, ***$P < 0.001$, ****$P < 0.0001$.

segmentation and tracking on all live-imaging sequences acquired (see Supplemental Digital Content 4, Figs. SDC_3-SDC_4 and Tables SDC_5-SDC_6, https://links.lww.com/RLI/B144, for full results). Compared with the manual analysis of GBCA-induced changes in mitochondrial area and length (Fig. SDC_3 A+B, https://links.lww.com/RLI/B144), the semi-automated segmentation consistently produced values that were 20% lower on average (except in noninflammatory negative controls), while still capturing the same trends under both inflammatory and noninflammatory conditions. In contrast, the aspect ratio values derived from the semi-automated analysis (Supplemental Digital Content 3, Table SDC_3, https://links.lww.com/RLI/B140) showed less agreement with the manual segmentation. At 50 mM gadopentetate, manual segmentation revealed a marked decrease in aspect ratio under both inflammatory and noninflammatory conditions (Fig. SDC_3C, https://links.lww.com/RLI/B144), which was not validated by the semi-automated tool. On the other hand, manual mitochondrial tracking generally validated the semi-automated analysis results on mitochondrial motility (Fig. SDC_4 A–C, https://links.lww.com/RLI/B144).

ICP-MS Quantifies Intratissue Gd Levels in Chronic Hippocampal Slices Ex Vivo

ICP-MS was performed to quantify the concentrations of Gd present within the slice tissue after prolonged GBCA exposure. Within hippocampal slices incubated with GBCAs at 10 and 50 mM for 48 hours, ICP-MS detected Gd levels between 81 and 612 µg/g, as shown in the Supplemental Table SDC_8 (Supplemental Digital Content 5, https://links.lww.com/RLI/B142), corresponding to about 3% to 8% of the originally applied GBCA dose. Slices incubated with 50 mM contained higher Gd levels (322.34 ± 193.89 µg/g) than those incubated with 10 mM (97.03 ± 19.73 µg/g). There was a trend for increased mean Gd concentrations (± TNFα) after gadopentetate compared with gadobutrol treatment at 10 mM. The inflammatory milieu (+TNFα) did not lead to consistent differences in Gd levels. Validating the method, samples from control groups (± TNFα) yielded Gd concentrations below the limit of quantification (< 0.16 ng/g) (Table SDC_8, Supplemental Digital Content 5, https://links.lww.com/RLI/B142).

DISCUSSION

In this study, we aimed to investigate whether inflammation promotes the duration and extent of hippocampal Gd retention following cumulative in vivo administration of GBCAs. We also sought to explore whether prolonged GBCA exposure in inflammatory and noninflammatory conditions alters mitochondrial dynamics in living neurons at biologically relevant, subcytotoxic concentrations. To this end, we assessed the kinetics and distribution patterns of Gd retention within the murine midbrain and, in particular, the hippocampus 1, 10, and 40 days after

repeated in vivo application of either linear gadopentetate or macrocyclic gadobutrol in EAE and HC mice using LA-ICP-ToF-MS. In addition, we investigated GBCA-induced changes in mitochondrial morphology and motility ex vivo in chronic murine organotypic hippocampal slice cultures following 48 hours of continuous exposure to gadopentetate or gadobutrol at 0.1, 1, 10, or 50 mM under both inflammatory and noninflammatory culture conditions. Total Gd content in slices after ex vivo GBCA exposure was further quantified by ICP-MS.

LA-ICP-ToF-MS revealed consistent spatial distribution patterns and temporal kinetics of Gd presence in EAE brains, including the hippocampus and DG, in agreement with previous findings demonstrating inflammation-promoted Gd retention in the cerebellum.[27] Gadobutrol resulted in diffuse Gd distribution that was efficiently cleared from both EAE and HC brains by day 40 p.f.i. In contrast, gadopentetate induced prolonged focal Gd retention with region-specific predilection sites in the hippocampus, isocortex, and basal ganglia. Within the hippocampus, Gd retention was pronounced in the granule cell layer of the DG and pyramidal layers of the cornu ammonis, particularly in EAE mice. Accordingly, cortical Gd concentrations at days 10 and 40 p.f.i. of gadopentetate were higher in EAE mice than in HC, consistent with sustained retention in a similar micromolar range as previously observed in the cerebellar cortex.[27]

Previous EPR analyses of cerebellar biopsies obtained from EAE mice 10 days p.f.i. of gadopentetate administration in vivo indicated that a fraction of retained Gd is present in a chemical environment distinct from the intact GBCA complex and in proximity to phosphorus (P)-containing molecules. This finding suggests partial in vivo Gd^{3+} release and formation of Gd species.[51] Additional evidence from MRI calibration experiments confirmed altered relaxometric properties of retained Gd after gadopentetate administration, likely reflecting interactions with inorganic ligands. In contrast, Gd signals after gadobutrol administration were consistent with intact complex-bound Gd.[51]

Following gadopentetate administration, Gd retention partially overlapped with Zn signals in the hippocampus, extending previous observations in the murine cerebellum,[27] and colocalized with Fe-rich regions, particularly within neuron-dense structures like the cornu ammonis and basal ganglia, with focal Gd hotspots most prominent in the globus pallidus. Although LA-ICP-ToF-MS does not provide submicrometric resolution, these observations are consistent with prior synchrotron x-ray spectroscopy data demonstrating ~160 nm Gd hotspots in Fe-rich dentate nuclei in HC and, particularly, EAE brains following linear GBCA administration.[50]

Together, these findings suggest that neuroinflammation-associated alterations in the tissue environment[75,76] promote in vivo dechelation and focal, long-lasting retention of kinetically less stable linear GBCAs in the CNS, particularly in regions rich in endogenous ions such as Fe, Zn, Mn, and P, whereas macrocyclic GBCAs mainly remain intact and follow compound-specific wash-out kinetics.[14,20,24,27,28,51,77–80]

In chronic hippocampal slice cultures, quantitative mitochondrial analyses under noninflammatory negative control conditions aligned well with previous findings, confirming the robustness of our semi-automated analysis approach.[58] Under noninflammatory conditions, both GBCAs induced comparable alterations in neuronal mitochondrial morphology and motility across concentrations, with good agreement between semi-automated and manual analyses. These findings align with observations of mitochondrial shortening and size reduction under oxidative stress in acute[81] and chronic hippocampal slice models.[58]

Mitochondrial dysfunction, ROS accumulation and impaired Ca^{2+} homeostasis during oxidative stress[41] have been linked to neuronal Gd-associated cytotoxicity (eg, due to competition for voltage-dependent Ca^{2+} channels),[27,82] particularly in the context of released Gd^{3+}.[82,83] Exposure to GBCAs has been shown to reduce mitochondrial membrane potential and oxidative capacity in neuronal cell lines, with effects observed for both linear and macrocyclic agents, but more pronounced at low millimolar to micromolar concentrations for kinetically less stable compounds such as gadopentetate than for gadobutrol.[84] In line with these findings, we show that both gadopentetate and gadobutrol induced mitochondrial alterations under noninflammatory conditions, suggesting that such effects in cell or tissue cultures do not necessarily require Gd^{3+} release. Instead, complex-bound Gd-mediated mechanisms, including interference with Ca^{2+}-regulated signaling pathways, intracellular compartmentalization, or potentially nonspecific cellular uptake,[85,86] likely contribute to the mitochondrial changes observed during prolonged ex vivo exposure.

At subcytotoxic concentrations, increased mitochondrial speed and displacement may reflect compensatory or adaptive responses to GBCA exposure, facilitating mitochondrial redistribution toward regions of increased energetic demand[87] or sites of quality control and turnover, such as mitochondria-lysosome contact regions. Although lysosomal markers were not assessed, the observed clustered and oscillatory mitochondrial movements are consistent with transient inter-organelle interactions described during mitochondrial quality control processes.[88,89]

Notably, no Gd^{3+} release was detected in recent ex vivo hippocampal slice culture EPR experiments following gadopentetate exposure at 1 mM.[51] However, ex vivo exposure to higher gadopentetate concentrations may additionally involve Gd^{3+} release, potentially contributing to the transition from adaptive mitochondrial responses to overt cytotoxicity. Accordingly, the marked reduction in mitochondrial speed as well as size and length (and rounding) observed at the highest gadopentetate concentration of 50 mM under noninflammatory conditions likely reflects mitochondrial impairment and fragmentation[90] at neurocytotoxic doses.[27]

Under inflammatory conditions, TNFα treatment alone reduced mitochondrial size without significantly affecting the motility. Gadopentetate induced dose-dependent morphologic alterations with maximal reductions at 50 mM and inflammation-dependent modulation of mitochondrial motility, culminating in maximal speed and displacement at high concentration. In contrast, gadobutrol caused milder inflammation-associated morphologic changes but consistently increased mitochondrial motility across doses, with inflammation further enhancing speed, displacement, and the fraction of motile mitochondria at higher concentrations. Overall, inflammation-dependent increases in mitochondrial motility at higher GBCA concentrations may reflect heightened mitochondrial stress in inflamed tissue or a short-lived compensatory mechanism preceding overt cytotoxicity.

In this context, the pro-inflammatory slice environment may additionally enhance Gd-induced toxicity by promoting cell death pathways,[91,92] or by reducing the chelate stability due to disturbances in the endogenous ion homeostasis[93] (ie, Ca^{2+} or Zn^{2+}[27]). Inflammatory modifications affecting structural and cell-associated macromolecules[75,76] could facilitate the binding of GBCAs to the surface of neurons, thereby promoting the potential cellular uptake[85] and toxic potential of GBCAs or formed Gd species.[86]

Importantly, total Gd content in the slices did not mirror the inflammation-dependent modulation of mitochondrial endpoints. Approximately 3% to 8% of the applied GBCA dose was detected within slices after 48 hours and this was not enhanced in the presence of TNFα. These values correspond to intratissue Gd concentrations in the low millimolar range. In contrast to these ex vivo findings, in vivo LA-ICP-ToF-MS revealed a clear stability-dependent pattern for long-term Gd retention, with persistent accumulation following linear GBCA administration, further enhanced under inflammatory conditions, whereas macrocyclic GBCA signals declined to near the detection limit over time.

Previous work using the same chronic slice model demonstrated that neuronal cell death started occurring at a gadopentetate treatment dose of 50 mM, particularly under inflammatory conditions.[27] Based on our ICP-MS quantification of slice Gd content, this corresponds to a mean intratissue Gd concentration of about 225 μg/g (~1.5 mM), and thus likely reflects the threshold of cytotoxicity in this ex vivo model. Following gadopentetate administration in vivo, peak Gd levels detected in the DG and hippocampus by LA-ICP-ToF-MS (~3 μg/g) remained below this ex vivo cytotoxic threshold. However, these concentrations correspond to an estimated low micromolar tissue range and are therefore within the measured or extrapolated order of magnitude potentially relevant to the mitochondrial alterations observed ex vivo at low (0.1 to 1 mM) to intermediate (10 mM) sub-cytotoxic GBCA exposure conditions. These findings suggest that repeated GBCA administration, particularly in the inflamed brain with focal hotspot accumulation, may result in cumulative Gd concentrations sufficient to perturb mitochondrial function in vivo. Consistent with this notion, Gd concentrations in human brain tissue following repeated linear GBCA administration range from ~0.5 to ~18.5 μg/g, even long after exposure,[69,70] whereas macrocyclic gadobutrol yields substantially lower levels (~36 ng/g).[71]

Together, these findings suggest that mitochondrial changes can occur after short-term GBCA exposure at biologically relevant intratissue Gd concentrations, potentially without substantial Gd^{3+} release. Under inflammatory conditions, mitochondrial responses are amplified despite comparable intratissue Gd levels, indicating that inflammation modulates cellular susceptibility to GBCA exposure rather than increasing Gd accumulation ex vivo. In contrast, long-term Gd retention in vivo is primarily determined by GBCA stability, with persistent accumulation following linear agents and efficient clearance of macrocyclic compounds. At high concentrations of linear GBCA exposure ex vivo, partial Gd^{3+} release may additionally exacerbate mitochondrial alterations, particularly under inflammatory conditions.

Therefore, the investigation of GBCA effects at clinically relevant concentrations is important, especially in the context of neuroinflammatory diseases, in which altered blood-brain barriers may facilitate the penetration of intact GBCA into the brain and the interaction with neurons. However, whether comparable mitochondrial effects may occur in human brain tissue under clinical exposure conditions remains to be established. Thus, the present findings should be interpreted with caution when extrapolating to the clinical setting. The experimental in vivo dosing regimen and ex vivo slice culture model were designed to investigate the biological effects of repeated (in vivo) and prolonged (ex vivo) GBCA exposure under controlled experimental conditions rather than to reproduce clinical exposure. Consequently, our findings primarily provide insight into how inflammation may influence GBCA retention and mitochondrial responses, rather than direct evidence of clinically relevant neurotoxicity. Accordingly, future studies should incorporate assessments of mitochondrial function, electrophysiological readouts, and cognitive and behavioral testing in vivo to better delineate potential mitotoxic and downstream neurotoxic effects of retained Gd.

Limitations

Repeated blinded manual analyses of mitochondrial morphology in chronic slices were complemented by semi-automated segmentation, revealing similar statistical significances for mitochondrial area and length but differences in aspect ratio. The consistently lower values for mitochondrial length and area obtained through semi-automated segmentation suggest that the level of automated threshold selection may be higher compared with manual evaluation, which could affect aspect ratio measurements. In manual morphologic analysis, thresholded particle outlines were carefully adjusted to match mitochondrial dimensions in the original images. Variability in image brightness and contrast, for example, due to differing proportions of neuronal somata and axons, may further contribute to these differences. Machine learning-based segmentation could improve accuracy, but this was beyond the scope of this study.

At the highest GBCA concentration tested ex vivo (50 mM), osmotic stress may have contributed to mitochondrial alterations, particularly following gadopentetate administration because of its higher osmolality. In addition, increased solution viscosity at this concentration cannot be excluded as a contributing factor, although neither parameter was assessed in the present study. Future experiments should therefore include an appropriate hyperosmolar control (eg, mannitol) to distinguish osmotic from GBCA-specific effects. However, such factors are unlikely to explain the concentration- and inflammation-dependent mitochondrial responses observed at lower, biologically relevant slice Gd concentrations.[84]

The experimental in vivo design, including frequency and daily GBCA doses, differed from applications in the clinical context; however, it adhered to previous publications.[27,50] The number of animals used for in vivo experiments, and the corresponding brain slices analyzed by LA-ICP-ToF-MS, was low ($n = 2$ mice per group and timepoint). Similarly, the ex vivo experiments were based on only 3 independent replicates per slice culture condition. These small sample sizes limited the statistical power to draw robust, translationally valid conclusions regarding hippocampal Gd retention in EAE and HC mouse brains, as well as the potential toxic effects of GBCAs on mitochondria. In addition, (LA-)ICP-MS cannot distinguish between intact GBCAs, free Gd^{3+}, or newly formed Gd-binding species, precluding conclusions regarding the chemical form of retained Gd.

CONCLUSIONS

Our combined in vivo and ex vivo findings in the hippocampus demonstrate that both linear gadopentetate and macrocyclic gadobutrol can induce measurable alterations in neuronal mitochondrial morphology and motility at biologically relevant, sub-cytotoxic intratissue Gd concentrations, particularly under inflammatory conditions. In chronic organotypic hippocampal slice cultures, these mitochondrial responses occurred independently of long-term Gd retention and were not restricted to linear GBCAs, indicating that acute and subacute mitochondrial effects can arise during GBCA exposure through complex-mediated mechanisms and inflammation-dependent modulation, without necessarily requiring substantial Gd^{3+} release.

In contrast, long-term in vivo Gd retention was observed exclusively for the linear GBCA gadopentetate and was promoted by neuroinflammation, whereas gadobutrol showed only temporary tissue Gd accumulation with near-complete washout. Whether transient mitochondrial alterations induced by macrocyclic GBCAs are fully reversible, and whether sustained Gd retention following linear GBCA administration leads to persistent or progressive mitochondrial dysfunction and associated cognitive impairment in neuroinflammatory diseases, remains to be determined.

Together, these findings suggest that short-term mitochondrial alterations during GBCA exposure and long-term Gd retention in vivo are determined by distinct but potentially interrelating mechanisms, underscoring the importance of inflammatory context, exposure duration, and GBCA stability when evaluating neurotoxic risks associated with repeated GBCA administration. Our data further emphasize the need to carefully distinguish between ex vivo and in vivo experimental approaches, as each may capture different but complementary aspects of GBCA- and Gd-associated effects.

ACKNOWLEDGMENTS

The authors gratefully acknowledge the contribution of the Advanced Medical BioImaging Core Facility of the Charité-Universitätsmedizin Berlin (AMBIO) to this study. They also thank Natascha Asselborn and Bibiane Seeger-Schwinge for their excellent technical support and engaging discussions during experimental procedures.

REFERENCES

1. Portaccio E, Magyari M, Havrdova EK, et al. Multiple sclerosis: emerging epidemiological trends and redefining the clinical course. *Lancet Reg Health Eur*. 2024;44:100977.
2. Di Filippo M, Portaccio E, Mancini A, et al. Multiple sclerosis and cognition: synaptic failure and network dysfunction. *Nat Rev Neurosci*. 2018;19:599–609.
3. Benedict RHB, Amato MP, DeLuca J, et al. Cognitive impairment in multiple sclerosis: clinical management, MRI, and therapeutic avenues. *Lancet Neurol*. 2020;19:860–871.
4. Montalban X, Lebrun-Frénay C, Oh J, et al. Diagnosis of multiple sclerosis: 2024 revisions of the McDonald criteria. *Lancet Neurol*. 2025; 24:850–865.
5. Wattjes MP, Ciccarelli O, Reich DS, et al. 2021 MAGNIMS-CMSC-NAIMS consensus recommendations on the use of MRI in patients with multiple sclerosis. *Lancet Neurol*. 2021;20:653–670.
6. Saade C, Bou-Fakhredin R, Yousem DM, et al. Gadolinium and multiple sclerosis: vessels, barriers of the brain, and glymphatics. *AJNR Am J Neuroradiol*. 2018;39:2168–2176.
7. Barkhof F, Reich DS, Oh J, et al. 2024 MAGNIMS-CMSC-NAIMS consensus recommendations on the use of MRI for the diagnosis of multiple sclerosis. *Lancet Neurol*. 2025;24:866–879.
8. Runge VM. Dechelation (transmetalation): consequences and safety concerns with the linear gadolinium-based contrast agents, in view of recent health care rulings by the EMA (Europe), FDA (United States), and PMDA (Japan). *Invest Radiol*. 2018;53:571–578.
9. Do QN, Lenkinski RE, Tircso G, et al. How the chemical properties of GBCAs influence their safety profiles in vivo. *Molecules*. 2021;27:58.
10. Hao D, Ai T, Goerner F, et al. MRI contrast agents: basic chemistry and safety. *J Magn Reson Imaging*. 2012;36:1060–1071.
11. Frenzel T, Lengsfeld P, Schirmer H, et al. Stability of gadolinium-based magnetic resonance imaging contrast agents in human serum at 37 degrees C. *Invest Radiol*. 2008;43:817–828.
12. Port M, Idee JM, Medina C, et al. Efficiency, thermodynamic and kinetic stability of marketed gadolinium chelates and their possible clinical consequences: a critical review. *BioMetals*. 2008;21:469–490.
13. Radbruch A. Gadolinium deposition in the brain: we need to differentiate between chelated and dechelated gadolinium. *Radiology*. 2018; 288:434–435.
14. Strzeminska I, Factor C, Jimenez-Lamana J, et al. Comprehensive speciation analysis of residual gadolinium in deep cerebellar nuclei in rats repeatedly administered with gadoterate meglumine or gadodiamide. *Invest Radiol*. 2022;57:283–292.
15. Errante Y, Cirimele V, Mallio CA, et al. Progressive increase of T1 signal intensity of the dentate nucleus on unenhanced magnetic resonance images is associated with cumulative doses of intravenously administered gadodiamide in patients with normal renal function, suggesting dechelation. *Invest Radiol*. 2014;49:685–690.
16. Weberling LD, Kieslich PJ, Kickingereder P, et al. Increased signal intensity in the dentate nucleus on unenhanced T1-weighted images after gadobenate dimeglumine administration. *Invest Radiol*. 2015;50:743–748.
17. Ramalho J, Castillo M, AlObaidy M, et al. High signal intensity in globus pallidus and dentate nucleus on unenhanced T1-weighted MR images: evaluation of two linear gadolinium-based contrast agents. *Radiology*. 2015;276:836–844.
18. Kanda T, Ishii K, Kawaguchi H, et al. High signal intensity in the dentate nucleus and globus pallidus on unenhanced T1-weighted MR images: relationship with increasing cumulative dose of a gadolinium-based contrast material. *Radiology*. 2014;270:834–841.
19. Robert P, Lehericy S, Grand S, et al. T1-weighted hypersignal in the deep cerebellar nuclei after repeated administrations of gadolinium-based contrast agents in healthy rats: difference between linear and macrocyclic agents. *Invest Radiol*. 2015;50:473–480.
20. Frenzel T, Apte C, Jost G, et al. Quantification and assessment of the chemical form of residual gadolinium in the brain after repeated administration of gadolinium-based contrast agents: comparative study in rats. *Invest Radiol*. 2017;52:396–404.
21. Jost G, Frenzel T, Boyken J, et al. Long-term excretion of gadolinium-based contrast agents: linear versus macrocyclic agents in an experimental rat model. *Radiology*. 2019;290:340–348.
22. U.S. Food and Drug Administration. FDA warns that gadolinium-based contrast agents (GBCAs) are retained in the body; requires new class warnings. 2017. Accessed July 12, 2025. https://www.fda.gov/drugs/fda-drug-safety-podcasts/fda-drug-safety-podcast-fda-warns-gadolinium-based-contrast-agents-gbcas-are-retained-body-requires.
23. Runge VM. Current research and development in the field of magnetic resonance contrast media. *Invest Radiol*. 2025;60:709–710.
24. Robert P, Fingerhut S, Factor C, et al. One-year retention of gadolinium in the brain: comparison of gadodiamide and gadoterate meglumine in a rodent model. *Radiology*. 2018;288:424–433.
25. Bussi S, Coppo A, Botteron C, et al. Differences in gadolinium retention after repeated injections of macrocyclic MR contrast agents to rats. *J Magn Reson Imaging*. 2018;47:746–752.
26. Frenzel T, Ulbrich HF, Pietsch H. The macrocyclic gadolinium-based contrast agents gadobutrol and gadoteridol show similar elimination kinetics from the brain after repeated intravenous injections in rabbits. *Invest Radiol*. 2021;56:341–347.
27. Anderhalten L, Silva RV, Morr A, et al. Different impact of gadopentetate and gadobutrol on inflammation-promoted retention and toxicity of gadolinium within the mouse brain. *Invest Radiol*. 2022; 57:677–688.
28. Bussi S, Coppo A, Celeste R, et al. Macrocyclic MR contrast agents: evaluation of multiple-organ gadolinium retention in healthy rats. *Insights Imaging*. 2020;11:11.
29. Granziera C, Reich DS. Gadolinium should always be used to assess disease activity in MS—yes. *Mult Scler*. 2020;26:765–766.
30. Loevner LA, Kolumban B, Hutóczki G, et al. Efficacy and safety of gadopiclenol for contrast-enhanced MRI of the central nervous system: the PICTURE randomized clinical trial. *Invest Radiol*. 2023;58:307–313.
31. Runge VM, Heverhagen JT. Diagnostic and technological advances in magnetic resonance (focusing on imaging technique and the gadolinium-based contrast media), computed tomography (focusing on photon counting CT), and ultrasound-state of the art. *Invest Radiol*. 2026;61: 145–147.
32. Frenzel T, Wels T, Pietsch H, et al. Recent developments and future perspectives in magnetic resonance imaging and computed tomography contrast media. *Invest Radiol*. 2026;61:214–223.
33. Roccatagliata L, Vuolo L, Bonzano L, et al. Multiple sclerosis: hyperintense dentate nucleus on unenhanced T1-weighted MR images is associated with the secondary progressive subtype. *Radiology*. 2009; 251:503–510.

34. Tedeschi E, Palma G, Canna A, et al. In vivo dentate nucleus MRI relaxometry correlates with previous administration of Gadolinium-based contrast agents. *Eur Radiol*. 2016;26:4577–4584.
35. Schlemm L, Chien C, Bellmann-Strobl J, et al. Gadopentetate but not gadobutrol accumulates in the dentate nucleus of multiple sclerosis patients. *Mult Scler*. 2017;23:963–972.
36. Malhotra A, LeSar B, Wu X, et al. Progressive T1 shortening of the dentate nucleus in patients with multiple sclerosis: result of multiple administrations of linear gadolinium contrast agents versus intrinsic disease. *AJR Am J Roentgenol*. 2018;211:1099–1105.
37. Kang H, Hii M, Le M, et al. Gadolinium deposition in deep brain structures: relationship with dose and ionization of linear gadolinium-based contrast agents. *AJNR Am J Neuroradiol*. 2018;39:1597–1603.
38. Eisele P, Szabo K, Ebert A, et al. Diffusion-weighted imaging of the dentate nucleus after repeated application of gadolinium-based contrast agents in multiple sclerosis. *Magn Reson Imaging*. 2019;58:1–5.
39. Stojanov DA, Aracki-Trenkic A, Vojinovic S, et al. Increasing signal intensity within the dentate nucleus and globus pallidus on unenhanced T1W magnetic resonance images in patients with relapsing-remitting multiple sclerosis: correlation with cumulative dose of a macrocyclic gadolinium-based contrast agent, gadobutrol. *Eur Radiol*. 2016;26:807–815.
40. Splendiani A, Perri M, Marsecano C, et al. Effects of serial macrocyclic-based contrast materials gadoterate meglumine and gadobutrol administrations on gadolinium-related dentate nuclei signal increases in unenhanced T1-weighted brain: a retrospective study in 158 multiple sclerosis (MS) patients. *Radiol Med*. 2018;123:125–134.
41. Mallio CA, Rovira À, Parizel PM, et al. Exposure to gadolinium and neurotoxicity: current status of preclinical and clinical studies. *Neuroradiology*. 2020;62:925–934.
42. Chehabeddine L, Al Saleh T, Baalbaki M, et al. Cumulative administrations of gadolinium-based contrast agents: risks of accumulation and toxicity of linear vs macrocyclic agents. *Crit Rev Toxicol*. 2019;49:262–279.
43. Radbruch A, Richter H, Bücker P, et al. Is small fiber neuropathy induced by gadolinium-based contrast agents? *Invest Radiol*. 2020;55:473–480.
44. Ayers-Ringler J, McDonald JS, Connors MA, et al. Neurologic effects of gadolinium retention in the brain after gadolinium-based contrast agent administration. *Radiology*. 2022;302:676–683.
45. Akai H, Okimoto N, Kato S, et al. Gadolinium Presence in the Brain After Gadolinium-based Contrast Agents: Evidence from Animal Behavioral Studies. *Invest Radiol*. 2026; Online ahead of print. doi:10.1097/RLI.0000000000001275
46. Yao X, Hu J, Wang G, et al. Deposition of gadolinium in the central and peripheral nervous systems and its effects on sensory, cognitive, and athletic implications after multiple injections of gadolinium-based contrast agents in rats. *AJNR Am J Neuroradiol*. 2024;45:1153–1161.
47. Solmaz V, Köse Özlece H, Fatih Bozkurt M, et al. Repeated gadoteric acid and gadobutrol exposure causes deterioration of behavior and memory functions in rats: MRI, histopathological and biochemical evidence. *Brain Res*. 2021;1754:147256.
48. Forslin Y, Shams S, Hashim F, et al. Retention of gadolinium-based contrast agents in multiple sclerosis: retrospective analysis of an 18-year longitudinal study. *AJNR Am J Neuroradiol*. 2017;38:1311–1316.
49. Forslin Y, Martola J, Bergendal Å, et al. Gadolinium retention in the brain: an mri relaxometry study of linear and macrocyclic gadolinium-based contrast agents in multiple sclerosis. *AJNR Am J Neuroradiol*. 2019;40:1265–1273.
50. Wang S, Hesse B, Roman M, et al. Increased retention of gadolinium in the inflamed brain after repeated administration of gadopentetate dimeglumine: a proof-of-concept study in mice combining ICP-MS and micro- and nano-SR-XRF. *Invest Radiol*. 2019;54:617–626.
51. Anderhalten L, Höfer N, ymnikova D D, Hahndorf J, Taupitz M, Traub H, Teutloff C, Infante-Duarte C, Bittl R, et al. EPR-based Assessment of Gadolinium-based Contrast Agent Retention and Gadolinium Transchelation in Inflamed Murine Brain. *Invest Radiol*. 2026; Online ahead of print. doi:10.1097/RLI.0000000000001280
52. Witte ME, Mahad DJ, Lassmann H, et al. Mitochondrial dysfunction contributes to neurodegeneration in multiple sclerosis. *Trends Mol Med*. 2014;20:179–187.
53. Barcelos IP, Troxell RM, Graves JS. Mitochondrial dysfunction and multiple sclerosis. *Biology (Basel)*. 2019;8:37.
54. Nikić I, Merkler D, Sorbara C, et al. A reversible form of axon damage in experimental autoimmune encephalomyelitis and multiple sclerosis. *Nat Med*. 2011;17:495–499.
55. Ohl K, Tenbrock K, Kipp M. Oxidative stress in multiple sclerosis: central and peripheral mode of action. *Exp Neurol*. 2016;277:58–67.
56. Kozin MS, Kulakova OG, Favorova OO. Involvement of mitochondria in neurodegeneration in multiple sclerosis. *Biochemistry*. 2018;83:813–830.
57. Bros H, Millward JM, Paul F, et al. Oxidative damage to mitochondria at the nodes of Ranvier precedes axon degeneration in ex vivo transected axons. *Exp Neurol*. 2014;261:127–135.
58. Ludwig R, Malla B, Höhrhan M, et al. Investigating the mitoprotective effects of S1P receptor modulators ex vivo using a novel semi-automated live imaging set-up. *Int J Mol Sci*. 2023;25:261.
59. Malla B, Cotten S, Ulshoefer R, et al. Teriflunomide preserves peripheral nerve mitochondria from oxidative stress-mediated alterations. *Ther Adv Chronic Dis*. 2020;11:2040622320944773.
60. Ulshöfer R, Bros H, Hauser AE, et al. Preventing axonal sodium overload or mitochondrial calcium uptake protects axonal mitochondria from oxidative stress-induced alterations. *Oxid Med Cell Longev*. 2022;2022:6125711.
61. Misgeld T, Kerschensteiner M, Bareyre FM, et al. Imaging axonal transport of mitochondria in vivo. *Nat Methods*. 2007;4:559–561.
62. Burger M, Hendriks L, Kaeslin J, et al. Characterization of inductively coupled plasma time-of-flight mass spectrometry in combination with collision/reaction cell technology—insights from highly time-resolved measurements. *J Anal At Spectrom*. 2019;34:135–146.
63. Paton C, Hellstrom J, Paul B, et al. Iolite: Freeware for the visualisation and processing of mass spectrometric data. *J Anal At Spectrom*. 2011;26:2508–2518.
64. Paul B, Petrus J, Savard D, et al. Time resolved trace element calibration strategies for LA-ICP-MS. *J Anal At Spectrom*. 2023;38:1995–2006.
65. Schweikert A, Theiner S, Wernitznig D, et al. Micro-droplet-based calibration for quantitative elemental bioimaging by LA-ICPMS. *Anal Bioanal Chem*. 2022;414:485–495.
66. Schannor M, Oelze M, Traub H, et al. Advancing biomarker research: in situ Cu isotope analysis in liver tumors by LA-MC-ICP-MS. *Anal Chem*. 2025;97:4425–4432.
67. Schneider CA, Rasband WS, Eliceiri KW. NIH Image to ImageJ: 25 years of image analysis. *Nat Methods*. 2012;9:671–675.
68. Rasschaert M, Couloumy E, Renard E, et al. Overall gadolinium exposure within the first 5 months after injection of human equivalent doses of gadopiclenol, gadoterate, or gadobutrol in healthy rats. *Invest Radiol*. 2025;60:753–767.
69. McDonald RJ, McDonald JS, Kallmes DF, et al. Intracranial gadolinium deposition after contrast-enhanced MR imaging. *Radiology*. 2015;275:772–782.
70. Kanda T, Fukusato T, Matsuda M, et al. Gadolinium-based contrast agent accumulates in the brain even in subjects without severe renal dysfunction: evaluation of autopsy brain specimens with inductively coupled plasma mass spectroscopy. *Radiology*. 2015;276:228–232.
71. El-Khatib AH, Radbruch H, Trog S, et al. Gadolinium in human brain sections and colocalization with other elements. *Neurol Neuroimmunol Neuroinflamm*. 2019;6:e515.
72. Thévenaz P, Ruttimann UE, Unser M. A pyramid approach to subpixel registration based on intensity. *IEEE Trans Image Process*. 1998;7:27–41.
73. Malla B, Niesner R, Hauser A, et al. Imaging and analysis of neuronal mitochondria in murine acute brain slices. *J Neurosci Methods*. 2022;372:109558.
74. Tinevez JY, Perry N, Schindelin J, et al. TrackMate: an open and extensible platform for single-particle tracking. *Methods*. 2017;115:80–90.
75. Wang S, Millward JM, Hanke-Vela L, et al. MR elastography-based assessment of matrix remodeling at lesion sites associated with clinical severity in a model of multiple sclerosis. *Front Neurol*. 2019;10:1382.
76. Silva RV, Biskup K, Zabala-Jouvin JK, et al. Brain inflammation induces alterations in glycosaminoglycan metabolism and subsequent changes in CS-4S and hyaluronic acid. *Int J Biol Macromol*. 2023;230:123214.
77. Strzeminska I, Factor C, Robert P, et al. Speciation analysis of gadolinium in the water-insoluble rat brain fraction after administration of gadolinium-based contrast agents. *Invest Radiol*. 2021;56:535–544.

78. Gianolio E, Bardini P, Arena F, et al. Gadolinium retention in the rat brain: assessment of the amounts of insoluble gadolinium-containing species and intact gadolinium complexes after repeated administration of gadolinium-based contrast agents. *Radiology*. 2017;285:839–849.
79. Le Fur M, Caravan P. The biological fate of gadolinium-based MRI contrast agents: a call to action for bioinorganic chemists. *Metallomics*. 2019;11:240–254.
80. Seeliger E, Hummel L, Frenzel T, et al. Comprehensive analysis of the spatial distribution of gadolinium, iron, manganese, and phosphorus in the brain of healthy rats after high-dose administrations of gadodiamide and gadobutrol. *Invest Radiol*. 2024;59:150–164.
81. Malla B, Liotta A, Bros H, et al. Teriflunomide preserves neuronal activity and protects mitochondria in brain slices exposed to oxidative stress. *Int J Mol Sci*. 2022;23:1538.
82. Feng X, Xia Q, Yuan L, et al. Impaired mitochondrial function and oxidative stress in rat cortical neurons: implications for gadolinium-induced neurotoxicity. *Neurotoxicology*. 2010;31:391–398.
83. Xia Q, Feng X, Huang H, et al. Gadolinium-induced oxidative stress triggers endoplasmic reticulum stress in rat cortical neurons. *J Neurochem*. 2011;117:38–47.
84. Bower DV, Richter JK, von Tengg-Kobligk H, et al. Gadolinium-based MRI contrast agents induce mitochondrial toxicity and cell death in human neurons, and toxicity increases with reduced kinetic stability of the agent. *Invest Radiol*. 2019;54:453–463.
85. Furlan C, Montarolo F, Di Gregorio E, et al. Analysis of the gadolinium retention in the experimental autoimmune encephalomyelitis (EAE) murine model of multiple sclerosis. *J Trace Elem Med Biol*. 2021;68:126831.
86. McDonald RJ, McDonald JS, Kallmes DF, et al. Gadolinium deposition in human brain tissues after contrast-enhanced MR imaging in adult patients without intracranial abnormalities. *Radiology*. 2017;285:546–554.
87. Licht-Mayer S, Campbell GR, Canizares M, et al. Enhanced axonal response of mitochondria to demyelination offers neuroprotection: implications for multiple sclerosis. *Acta Neuropathol*. 2020;140:143–167.
88. Picca A, Calvani R, Coelho-Junior HJ, et al. Inter-organelle membrane contact sites and mitochondrial quality control during aging: a geroscience view. *Cells*. 2020;9:598.
89. Cisneros J, Belton TB, Shum GC, et al. Mitochondria-lysosome contact site dynamics and misregulation in neurodegenerative diseases. *Trends Neurosci*. 2022;45:312–322.
90. Wen P, Sun Z, Gou F, et al. Oxidative stress and mitochondrial impairment: key drivers in neurodegenerative disorders. *Ageing Res Rev*. 2025;104:102667.
91. Fresegna D, Bullitta S, Musella A, et al. Re-examining the role of TNF in MS pathogenesis and therapy. *Cells*. 2020;9:2290.
92. Aktas O, Smorodchenko A, Brocke S, et al. Neuronal damage in autoimmune neuroinflammation mediated by the death ligand TRAIL. *Neuron*. 2005;46:421–432.
93. Tweedle MF, Wedeking P, Kumar K. Biodistribution of radiolabeled, formulated gadopentetate, gadoteridol, gadoterate, and gadodiamide in mice and rats. *Invest Radiol*. 1995;30:372–380.

